Interaction and Multiscale Mechanics, Vol. 3, No. 2 (2010) 123-143
DOI: http://dx.doi.org/10.12989/imm.2010.3.2.123

Improved Element-Free Galerkin method (IEFG) for solving three-dimensional elasticity problems

Zan Zhang[1] and K.M. Liew[2]*

[1]*Shanghai Institute of Applied Mathematics and Mechanics, Shanghai University, Shanghai 200072, China*
[2]*Department of Building and Construction, City University of Hong Kong, Tat Chee Avenue, Kowloon, Hong Kong SAR*

(Received March 30, 2010, Accepted May 28, 2010)

Abstract. The essential idea of the element-free Galerkin method (EFG) is that moving least-squares (MLS) approximation are used for the trial and test functions with the variational principle (weak form). By using the weighted orthogonal basis function to construct the MLS interpolants, we derive the formulae for an improved element-free Galerkin (IEFG) method for solving three-dimensional problems in linear elasticity. There are fewer coefficients in improved moving least-squares (IMLS) approximation than in MLS approximation. Also fewer nodes are selected in the entire domain with the IEFG method than is the case with the conventional EFG method. In this paper, we selected a few example problems to demonstrate the applicability of the method.

Keywords: weighted orthogonal function; Improved moving least-squares (IMLS) approximation; Element-free Galerkin (EFG) method; Improved element-free Galerkin (IEFG) method; 3D elastic problem.

1. Introduction

A number of meshless methods have been developed in recent years, and have achieved remarkable progress in computational mechanics. The main objective of such methods is to eliminate, or at least to alleviate, the difficulty of meshing and remeshing the entire problem domain by simply adding or deleting nodes. The main difference between meshless and conventional numerical methods is the way in which the shape function is formulated. However, once this function has been obtained, the meshless method, the finite element method (FEM), and the boundary element method (BEM) all use the same procedure to form the equations needed to obtain the solution to a problem (Belytschko *et al*. 1996).

There are several meshless methods: the diffuse element method (Nayroles *et al*. 1992), the element-free Galerkin (EFG) method (Belytschko *et al*. 1994), the Hp clouds method (Duarte and Oden 1995), the meshless local Petrov-Galerkin method (Atluri and Zhu 1998), the reproducing kernel particle method (Liu *et al*. 1995), the radial point interpolation method (Liew and Chen 2004a, Liew and Chen 2004b, Liew and Chen 2004c), the complex variable meshless method (Liew *et al*. 2007), the boundary element-free method (Kitipornchai *et al*. 2005, Liew *et al*. 2005, Sun *et*

* Corresponding author, Chair Professor, E-mail: kmliew@cityu.edu.hk

al. 2006, Liew *et al*. 2006), and the moving least-squares differential quadrature meshfree method (Liew *et al*. 2003, Liew *et al*. 2004) and others (Hu *et al*. 2009, Matsubara and Yagawa 2009, Wu and Koishi 2009, Wang and Wu 2008). All of these methods evaluate the field variables based entirely on a set of discrete nodes and require no predefined nodal connectivity (Liu 2003). As there is no need to create a mesh, and the nodes can be created by a computer in a fully automated manner, the time that an engineer would have spent on conventional mesh generation is minimized.

The EFG method, which is one of the most promising meshless methods, was developed based on the discrete element method (DEM). It essentially has two aspects: moving least squares (MLS) approximation is used for the construction of the shape function, and the Galerkin weak form is employed to develop the discretized system equation (Liu 2003). MLS approximation was developed from the conventional least-squares method, and in practical numerical processes it essentially involves the application of the conventional method to every selected point. A disadvantage of the conventional least-squares method is that the final algebra equations system is sometimes ill-conditioned. Hence, this ill-conditioned algebra equations system must be solved in MLS approximation. However, it is difficult to determine which system is ill-conditioned, as no methods in mathematical theory judge whether a system is ill-conditioned before the equation is solved. Thus, it is sometimes impossible to obtain a good, or even correct, numerical solution. This drawback can be avoided by using the improved moving least-squares (IMLS) technique to obtain the approximation function. In this type of approximation, an orthogonal function system with a weight function is used as the basis function. The algebra equations system in IMLS approximation is not ill-conditioned, and it can be solved without the need to derive the inverse matrix.

Based on IMLS approximation and the EFG method, an improved element-free Galerkin (IEFG) method is formulated. The IEFG method is used in this paper to study three-dimensional (3D) elastic problems. Several numerical examples for the elastic problems are presented to evaluate the accuracy and efficiency of the proposed technique.

2. Improved Moving Least-Squares (IMLS) approximation

In the EFG method, MLS approximation is employed for the construction of the shape function. The MLS approximation is useful because the approximated field function is continuous and smooth in the entire problem domain, and it is capable of producing an approximation with the desired order of consistency (Liu 2003).

2.1 MLS approximation function

Let $u(\boldsymbol{x})$ be the function of the field variable defined in the domain Ω. The MLS approximation of $u(\boldsymbol{x})$ at point $\boldsymbol{x}$ is denoted $u^h(\boldsymbol{x})$, and the trial function is

$$u^h(\mathbf{x}) = \sum_{i=1}^{m} p_i(\mathbf{x}) a_i(\mathbf{x}) = \mathbf{p}^{\mathrm{T}}(\mathbf{x})\mathbf{a}(\mathbf{x}) \tag{1}$$

where $\boldsymbol{p}(\boldsymbol{x})$ is a vector of basis functions that consists of monomials of the lowest order to ensure minimum completeness, m is the number of terms of the monomials, and $\boldsymbol{a}(\boldsymbol{x})$ is a vector of coefficients given by

$$\boldsymbol{a}^{\mathrm{T}}(x) = (a_0(x), a_1(x), \ldots, a_m(x)) \tag{2}$$

which are functions of $\boldsymbol{x}$.

In the three dimensions, the following basis can be chosen

$$\boldsymbol{p}^{T}(\boldsymbol{x}) = (1, x, y, z) \qquad (m = 4, \text{ linear basis) or} \tag{3}$$

$$\boldsymbol{p}^{T}(\boldsymbol{x}) = (1, x, y, z, xy, yz, zx, x^2, y^2, z^2) \qquad (m = 10, \text{ quadratic basis}) \tag{4}$$

The local approximation at $\boldsymbol{x}$, as described by Lancaster and Salkauskas (1981), is

$$u^h(\mathbf{x}, \bar{\mathbf{x}}) = \sum_{i=1}^{m} p_i(\bar{\mathbf{x}}) a_i(\mathbf{x}) = \mathbf{p}^{\mathrm{T}}(\bar{\mathbf{x}})\mathbf{a}(\mathbf{x}) \tag{5}$$

where $\bar{\boldsymbol{x}}$ is the point in the local approximation of $\boldsymbol{x}$.

To obtain the local approximation of the function $u(\boldsymbol{x})$, the difference between it and the local approximation $u^h(\boldsymbol{x})$ must be minimized by a weighted least-squares method.

Define the function

$$J = \sum_{I=1}^{n} w(\boldsymbol{x} - \boldsymbol{x}_I)[u^h(\boldsymbol{x}, \boldsymbol{x}_I) - u(\boldsymbol{x}_I)]^2 = \sum_{I=1}^{n} w(\boldsymbol{x} - \boldsymbol{x}_I)\left[\sum_{i=1}^{m} p_i(\boldsymbol{x}_I) \cdot a_i(\boldsymbol{x}) - u(\boldsymbol{x}_I)\right]^2 \tag{6}$$

where $w(\boldsymbol{x} - \boldsymbol{x}_I)$ is a weight function with a domain of influence, and $\boldsymbol{x}_I (I = 1, 2, \ldots, n)$ are the nodes with domains of influence that cover point $\boldsymbol{x}$.

Eq. (6) can be written as

$$\boldsymbol{J} = (\boldsymbol{P}\boldsymbol{a} - \boldsymbol{u})^T \boldsymbol{W}(\boldsymbol{x})(\boldsymbol{P}\boldsymbol{a} - \boldsymbol{u}) \tag{7}$$

where

$$\boldsymbol{u}^{\mathrm{T}} = (u_1, u_2, \ldots, u_n) \tag{8}$$

$$\boldsymbol{P} = \begin{bmatrix} p_1(x_1) & p_2(x_1) & \cdots & p_m(x_1) \\ p_1(x_2) & p_2(x_2) & \cdots & p_m(x_2) \\ \vdots & \vdots & \ddots & \vdots \\ p_1(x_n) & p_2(x_n) & \cdots & p_m(x_n) \end{bmatrix} \quad \text{and} \tag{9}$$

$$\boldsymbol{W}(\boldsymbol{x}) = \begin{bmatrix} w(\boldsymbol{x} - \boldsymbol{x}_1) & 0 & \cdots & 0 \\ 0 & w(\boldsymbol{x} - \boldsymbol{x}_2) & \cdots & 0 \\ \vdots & \vdots & \ddots & \vdots \\ 0 & 0 & \cdots & w(\boldsymbol{x} - \boldsymbol{x}_n) \end{bmatrix} \tag{10}$$

The minimization condition requires that

$$\frac{\partial J}{\partial \boldsymbol{a}} = 0 \tag{11}$$

that results in the equation system

$$\boldsymbol{A}(\boldsymbol{x})\boldsymbol{a}(\boldsymbol{x}) = \boldsymbol{B}(\boldsymbol{x})\boldsymbol{u} \tag{12}$$

where matrices $\boldsymbol{A}(\boldsymbol{x})$ and $\boldsymbol{B}(\boldsymbol{x})$ are

$$\boldsymbol{A}(\boldsymbol{x}) = \boldsymbol{P}^{\mathrm{T}}\boldsymbol{W}(\boldsymbol{x})\boldsymbol{P} \text{ and} \tag{13}$$

$$\boldsymbol{B}(\boldsymbol{x}) = \boldsymbol{P}^{\mathrm{T}}\boldsymbol{W}(\boldsymbol{x}) \tag{14}$$

in which $\boldsymbol{u}$ is the vector that collects the nodal parameters of the field variables for all of the nodes in the support domain.

From Eq. (12), we obtain

$$\boldsymbol{a}(\boldsymbol{x}) = \boldsymbol{A}^{-1}(\boldsymbol{x})\boldsymbol{B}(\boldsymbol{x})\boldsymbol{u} \tag{15}$$

The expression of the local approximation $u^h(\boldsymbol{x})$ is thus

$$u^h(\boldsymbol{x}) = \boldsymbol{\Phi}(\boldsymbol{x})\boldsymbol{u} = \sum_{I=1}^{n} \Phi_I(\boldsymbol{x})u_I \tag{16}$$

where $\boldsymbol{\Phi}(\boldsymbol{x})$ is the MLS shape function and

$$\boldsymbol{\Phi}(\boldsymbol{x}) = (\Phi_1(\boldsymbol{x}), \Phi_2(\boldsymbol{x}), \ldots, \Phi_n(\boldsymbol{x})) = \boldsymbol{P}^{\mathrm{T}}(\boldsymbol{x})\boldsymbol{A}^{-1}(\boldsymbol{x})\boldsymbol{B}(\boldsymbol{x}) \tag{17}$$

2.2 The IMLS procedure

In MLS approximation, Eq. (12) is sometimes ill-conditioned, even in the presence of a singular phenomenon. Thus, it is difficult to obtain a correct numerical solution. To overcome this, the weighted orthogonal basis functions can be employed to present the IMLS approximation (Matsubara and Yagawa 2009).

For $\forall f(\boldsymbol{x})$, $g(\boldsymbol{x}) \in span(\boldsymbol{p})$, we define

$$(f, g) = \sum_{I=1}^{n} w(\boldsymbol{x} - \boldsymbol{x}_I)f(\boldsymbol{x}_I)g(\boldsymbol{x}_I) \tag{18}$$

and then (f, g) is an inner product, and $span(\boldsymbol{p})$ is a Hilbert space.

In the Hilbert space $span(\boldsymbol{p})$, for the set of points $\{\boldsymbol{x}_i\}$ and the weight functions $\{w_i\}$, if the functions $p_1(\boldsymbol{x}), p_2(\boldsymbol{x}), \ldots, p_m(\boldsymbol{x})$ satisfy the conditions

$$(p_k, p_j) = \sum_{i=1}^{n} w_i p_k(\boldsymbol{x}_i)p_j(\boldsymbol{x}_i) = \begin{cases} 0 & k \neq j \\ A_k & k = j \end{cases} \quad (k, j = 1, 2, \ldots, m) \tag{19}$$

then the function set $p_1(\boldsymbol{x}), p_2(\boldsymbol{x}), \ldots, p_m(\boldsymbol{x})$ is called a weighted orthogonal function set with weight functions $\{w_i\}$ at points $\{\boldsymbol{x}_i\}$. If $p_1(\boldsymbol{x}), p_2(\boldsymbol{x}), \ldots, p_m(\boldsymbol{x})$ are polynomials, then the function set $p_1(\boldsymbol{x}), p_2(\boldsymbol{x}), \ldots, p_m(\boldsymbol{x})$ is called a weighted orthogonal polynomials set with weight functions $\{w_i\}$ at points $\{\boldsymbol{x}_i\}$.

From Eq. (18), Eq. (12) can be written as

$$\begin{bmatrix} (p_1,p_1) & (p_1,p_2) & \cdots & (p_1,p_m) \\ (p_2,p_1) & (p_2,p_2) & \cdots & (p_2,p_m) \\ \vdots & \vdots & \ddots & \vdots \\ (p_m,p_1) & (p_m,p_2) & \cdots & (p_m,p_m) \end{bmatrix} \begin{bmatrix} a_1(\boldsymbol{x}) \\ a_2(\boldsymbol{x}) \\ \vdots \\ a_m(\boldsymbol{x}) \end{bmatrix} = \begin{bmatrix} (p_1,u_I) \\ (p_2,u_I) \\ \vdots \\ (p_m,u_I) \end{bmatrix} \tag{20}$$

If the basis function set $p_i(\boldsymbol{x}) \in span(\boldsymbol{p})$, $i = 1, 2, \ldots, m$ is a weighted orthogonal function set at points $\{\boldsymbol{x}_i\}$, i.e., if

$$(p_i, p_j) = 0 \qquad (i \neq j) \tag{21}$$

then Eq. (20) becomes

$$\begin{bmatrix} (p_1,p_1) & 0 & \cdots & 0 \\ 0 & (p_2,p_2) & \cdots & 0 \\ \vdots & \vdots & \ddots & \vdots \\ 0 & 0 & \cdots & (p_m,p_m) \end{bmatrix} \begin{bmatrix} a_1(\boldsymbol{x}) \\ a_2(\boldsymbol{x}) \\ \vdots \\ a_m(\boldsymbol{x}) \end{bmatrix} = \begin{bmatrix} (p_1,u_I) \\ (p_2,u_I) \\ \vdots \\ (p_m,u_I) \end{bmatrix} \tag{22}$$

We can then obtain the coefficients $a_i(\boldsymbol{x})$ directly, as follows

$$a_i(\boldsymbol{x}) = \frac{(p_i, u_I)}{(p_i, p_i)} \quad (i = 1, 2, \ldots, m) \tag{23}$$

i.e.,

$$\boldsymbol{a}(\boldsymbol{x}) = \overline{\boldsymbol{A}}(\boldsymbol{x})\boldsymbol{B}(\boldsymbol{x})\boldsymbol{u} \tag{24}$$

where

$$\overline{\boldsymbol{A}}(\boldsymbol{x}) = \begin{bmatrix} \dfrac{1}{(p_1,p_1)} & 0 & \cdots & 0 \\ 0 & \dfrac{1}{(p_2,p_2)} & \cdots & 0 \\ \vdots & \vdots & \ddots & \vdots \\ 0 & 0 & \cdots & \dfrac{1}{(p_m,p_m)} \end{bmatrix} \tag{25}$$

From Eqs. (23) and (5), the expression of the approximation function $u^h(\boldsymbol{x})$ is

$$u^h(\boldsymbol{x}) = \overline{\boldsymbol{\Phi}}(\boldsymbol{x})\boldsymbol{u} = \sum_{I=1}^{n} \overline{\Phi}_I(\boldsymbol{x}) u_I \tag{26}$$

where $\overline{\boldsymbol{\Phi}}(\boldsymbol{x})$ is the shape function and

$$\overline{\boldsymbol{\Phi}}(\boldsymbol{x}) = (\overline{\Phi}_1(\boldsymbol{x}), \overline{\Phi}_2(\boldsymbol{x}), \ldots, \overline{\Phi}_n(\boldsymbol{x})) = \boldsymbol{P}^{\mathrm{T}}(\boldsymbol{x})\overline{\boldsymbol{A}}(\boldsymbol{x})\boldsymbol{B}(\boldsymbol{x}) \tag{27}$$

This is an IMLS approximation in which the coefficients $a_i(\boldsymbol{x})$ are obtained. It is impossible to yield an ill-conditioned or singular equations system, and we can thus obtain the correct solution.

From Eq. (27), we have

$$\overline{\Phi}_I(\boldsymbol{x}) = \sum_{j=1}^{m} p_j(\boldsymbol{x})[\overline{\boldsymbol{A}}(\boldsymbol{x})\boldsymbol{B}(\boldsymbol{x})]_{jI} \tag{28}$$

which represents the shape function of the IMLS approximation corresponding to node I. Then, the partial derivatives of $\overline{\Phi}_I(\boldsymbol{x})$ can be obtained as

$$\overline{\Phi}_{I,i}(\boldsymbol{x}) = \sum_{j=1}^{m} [p_{j,i}(\overline{\boldsymbol{A}}\boldsymbol{B})_{jI} + p_j(\overline{\boldsymbol{A}}_{,i}\boldsymbol{B} + \overline{\boldsymbol{A}}\boldsymbol{B}_{,i})_{jI}] \tag{29}$$

The weighted orthogonal basis function set $\boldsymbol{p} = (p_i)$ can be formed with the Schmidt method

$$\begin{aligned} p_1 &= 1 \\ p_i &= r^{i-1} - \sum_{k=1}^{i-1} \frac{(r^{i-1}, p_k)}{(p_k, p_k)} p_k, \qquad i = 2, 3, \ldots \end{aligned} \tag{30}$$

or can be expressed as

$$\begin{aligned} p_1 &= 1 \\ p_2 &= r - a_2 \\ p_i &= (r - a_i)p_{i-1} - b_i p_{i-2}, \qquad i = 3, 4, \ldots \end{aligned} \tag{31}$$

where

$$a_i = \frac{(rp_{i-1}, p_{i-1})}{(p_{i-1}, p_{i-1})} \tag{32}$$

$$b_i = \frac{(p_{i-1}, p_{i-1})}{(p_{i-2}, p_{i-2})} \tag{33}$$

and $r = \sqrt{x_1^2 + x_2^2 + x_3^2}$, or $r = x_1 + x_2 + x_3$ for 3D problems.

Furthermore, using the Schmidt method, the weighted orthogonal basis function set $\boldsymbol{p} = (p_i)$ can be constructed from the monomial basis function. For example, for the monomial basis function

$$\bar{\boldsymbol{p}} = (\bar{p}_i) = (1, x_1, x_2, x_3, x_1x_2, x_1x_3, x_2x_3, x_1^2, x_2^2, x_3^2 \ldots) \tag{34}$$

the weighted orthogonal basis function set can be generated as

$$p_i = \bar{p}_i - \sum_{k=1}^{i-1} \frac{(\bar{p}_i, p_k)}{(p_k, p_k)} p_k, \qquad i = 1, 2, 3, \ldots \tag{35}$$

When the weighted orthogonal basis functions (30) and (31) are used, there are fewer coefficients in the trial function. Therefore fewer nodes are needed in the domain of influence in IMLS approximation than in MLS approximation.

2.3 Weight function

The weight function used in Eq. (6) through Eq. (17) plays an important role in the EFG method.

This function should be non-zero over only a small neighborhood of x_I to generate a set of sparse discrete equations.

Define $d_I = \|x - x_I\|$ and $r = d_I / d_{mI}$, where d_{mI} is the size of the domain of influence of the I^{th} node. Then, the weight function can be written as a function of normalized radius r. In this paper, we use the cubic spline weight function

$$w(x - x_I) \equiv w(r) = \begin{cases} \frac{2}{3} - 4r^2 + 4r^3 & r \le \frac{1}{2} \\ \frac{4}{3} - 4r + 4r^2 - \frac{4}{3}r^3 & \frac{1}{2} < r \le 1 \\ 0 & r > 1 \end{cases} \tag{36}$$

The size of the domain of influence at a node, d_{mI}, is computed by

$$d_{mI} = d_{\max} c_I \tag{37}$$

where d_{max} is a scaling parameter that is typically 2.0-4.0 for a static analysis, and distance c_I is determined by searching for enough neighbor nodes to allow **A** to be regular, i.e., invertible. Due to Eq. (29), we must compute the spatial derivative of the weight function as

$$\frac{dw_I}{dx} = \frac{dw_I}{dr}\frac{dr}{dx} = \begin{cases} (-8r + 12r^2) sign(x - x_I) & for\ r \le \frac{1}{2} \\ (-4 + 8r - 4r^2) sign(x - x_I) & for\ \frac{1}{2} < r \le 1 \\ 0 & for\ r > 1 \end{cases} \tag{38}$$

3. IEFG method for 3D elasticity problems

3.1 Governing equations

Consider a continuum of 3D elastic solids with volume Ω and surface boundary Γ, as shown in Fig. 1. The governing equation of equilibrium is

$$\nabla \cdot \boldsymbol{\sigma} + \mathbf{b} = 0 \qquad \text{in } \Omega \tag{39}$$

where

$$\boldsymbol{\sigma} = \mathbf{D}\varepsilon,\ \varepsilon = \nabla_s \mathbf{u} \tag{40}$$

In the above, Ω is the domain of the body, $\boldsymbol{\sigma}$ is the stress tensor, ε is the strain, $\mathbf{b}$ is the body force per unit volume, $\mathbf{D}$ is a matrix of material constants, $\mathbf{u}$ is the displacement, $\nabla \cdot$ is the divergence operator, and ∇_s is the symmetric gradient operator.

The boundary conditions are

$$\mathbf{u} = \bar{\mathbf{u}},\ \text{on} \quad \Gamma_u \tag{41}$$

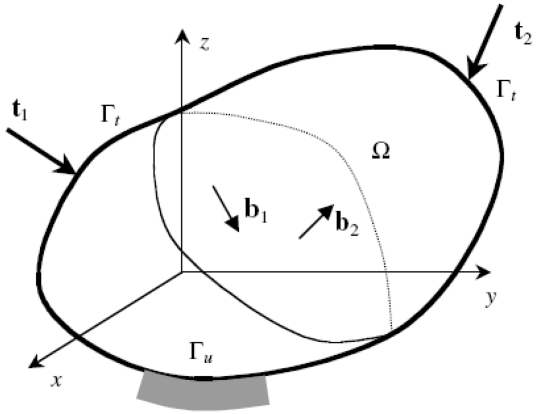

Fig. 1 A continuum of Solid subjected to force

and

$$\boldsymbol{\sigma} \cdot \mathbf{n} = \bar{\mathbf{t}}, \quad \text{on} \quad \Gamma_t \tag{42}$$

where $\bar{\mathbf{u}}$ is the prescribed displacement on essential boundary Γ_u, $\bar{\mathbf{t}}$ is the prescribed traction on natural boundary Γ_t, and $\mathbf{n}$ is the unit normal outward to the domain boundary. Also

$$\bar{\mathbf{u}} = \begin{bmatrix} \bar{u}_x \\ \bar{u}_y \\ \bar{u}_z \end{bmatrix} \text{ and} \tag{43}$$

$$\mathbf{D} = \frac{2G}{(1-2\nu)} \begin{bmatrix} 1-\nu & \nu & \nu & 0 & 0 & 0 \\ \nu & 1-\nu & \nu & 0 & 0 & 0 \\ \nu & \nu & 1-\nu & 0 & 0 & 0 \\ 0 & 0 & 0 & \frac{1-2\nu}{2} & 0 & 0 \\ 0 & 0 & 0 & 0 & \frac{1-2\nu}{2} & 0 \\ 0 & 0 & 0 & 0 & 0 & \frac{1-2\nu}{2} \end{bmatrix} \text{ for tridimensional stress.} \tag{44}$$

3.2 The Galerkin weak form

The use of MLS approximation produces shape functions that do not possess the Kronecker delta function property, i.e., $\phi_I(x_J) \neq \delta_{IJ}$, and therefore $u^h(x_J) \neq u_J$. This implies that essential boundary conditions cannot be imposed in the same way as in the FEM (Liu 2003). In this paper, we use penalty factors to enforce these conditions. The use of the penalty method produces equation systems of the same dimensions as those produced by FEM for the same number of nodes, and the modified stiffness matrix is still positively defined (Liu 2003). Moreover, the symmetry and

bandness of the system matrix are preserved.

In the IEFG method, the essential boundary conditions that need to be enforced have the form

$$\sum_{I}^{n} \phi_I(x)\mathbf{u}_I = \bar{\mathbf{u}}(x) \qquad \text{on} \qquad \Gamma_u \tag{45}$$

where $\bar{\mathbf{u}}(x)$ is the prescribed displacement on the essential boundary.

Now, consider the problem stated in Eqs. (39)-(42). We introduce a penalty factor to penalize the difference between the displacement of the MLS approximation and the prescribed displacement on the essential boundary. The constrained Galerkin weak form using the penalty method becomes

$$\Pi = \frac{1}{2}\int_{\Omega} \nabla \mathbf{u}^{\mathrm{T}} \mathbf{D} \nabla \mathbf{u} d\Omega - \int_{\Omega} \mathbf{u}^{\mathrm{T}} \cdot \mathbf{b} \mathrm{d}\Omega - \int_{\Gamma_t} \mathbf{u}^{\mathrm{T}} \cdot \bar{\mathbf{t}} d\Gamma + \frac{1}{2}\int_{\Gamma_u} (\mathbf{u} - \bar{\mathbf{u}}) \cdot (\alpha \cdot \boldsymbol{S}) \cdot (\mathbf{u} - \bar{\mathbf{u}}) d\Gamma \tag{46}$$

where $\alpha = (\alpha_1, \alpha_2, \ldots, \alpha_k)$ is a diagonal matrix of the penalty factor and $k = 3$ for 3D cases. The penalty factors $\alpha_i (i = 1, \ldots, k)$ can be a function of the coordinates and different from one another, even though in practice we often assign them the identical constant of a large positive number, which can be chosen with the following way (Liu 2003)

$$\alpha = 1.0 \times 10^{5-8} \times E \text{ and} \tag{47}$$

$$\boldsymbol{S} = \begin{bmatrix} s_1 & 0 & 0 \\ 0 & s_2 & 0 \\ 0 & 0 & s_3 \end{bmatrix} \tag{48}$$

When there are displacement restrictions along the direction of x_1 (or x_2, x_3), s_1 (or s_2, s_3) is, correspondingly, equal to one; otherwise, it is equal to zero.

Substituting Eqs. (26) (which is the approximation function of the IMLS), (47) and (48) into Eq. (46) yields the following total potential

$$\Pi = \frac{1}{2}\mathbf{u}^{\mathrm{T}}(\mathbf{K} + \mathbf{K}^{\alpha})\mathbf{u} - \mathbf{u}^{\mathrm{T}} \cdot (\mathbf{F} + \mathbf{F}^{\alpha}) \tag{49}$$

Invoking the stationary condition of Π, i.e., $\delta\Pi = 0$, gives the following linear system of $\mathbf{u}$.

$$\lfloor \mathbf{K} + \mathbf{K}^{\alpha} \rfloor \mathbf{u} = \mathbf{F} + \mathbf{F}^{\alpha} \tag{50}$$

where

$$\mathbf{K}_{IJ} = \int_{\Omega} \mathbf{B}_i^{\mathrm{T}} \mathbf{D} \mathbf{B}_j d\Omega, \qquad i, j = 1, 2, 3, \ldots, n \text{ and} \tag{51}$$

$$\mathbf{F}_I = \int_{\Gamma_\sigma} \bar{\boldsymbol{\Phi}}_I^{\mathrm{T}} \bar{\mathbf{t}} \mathrm{d}\Gamma + \int_{\Omega} \bar{\boldsymbol{\Phi}}_I^{\mathrm{T}} \mathbf{b} \mathrm{d}\boldsymbol{\Omega} \tag{52}$$

The additional matrix $\mathbf{K}^{\alpha}$ is the global penalty matrix assembled using the nodal matrix defined by

$$\mathbf{K}_{IJ}^{\alpha} = \alpha \int_{\Gamma_u} \bar{\boldsymbol{\Phi}}_I^{\mathrm{T}} \boldsymbol{S} \bar{\boldsymbol{\Phi}}_J d\Gamma \tag{53}$$

The vector $\mathbf{F}^{\alpha}$ is caused by the essential boundary condition, and its nodal vector takes the form

$$\mathbf{F}_I^{\alpha} = \alpha \int_{\Gamma_u} \bar{\boldsymbol{\Phi}}_I^{\mathrm{T}} \boldsymbol{S} \bar{\mathbf{u}} d\Gamma \tag{54}$$

with

$$\mathbf{B}_I = \begin{bmatrix} \overline{\Phi}_{I,x} & 0 & 0 \\ 0 & \overline{\Phi}_{I,y} & 0 \\ 0 & 0 & \overline{\Phi}_{I,z} \\ 0 & \overline{\Phi}_{I,z} & \overline{\Phi}_{I,y} \\ \overline{\Phi}_{I,z} & 0 & \overline{\Phi}_{I,x} \\ \overline{\Phi}_{I,y} & \overline{\Phi}_{I,x} & 0 \end{bmatrix} \tag{55}$$

4. Numerical results and discussion

4.1 Convergence analysis and error estimation

A convergence study of the proposed method is carried out by analyzing the final function values under different discretization schemes and different scaling factors for the nodes of the study field.

For error estimation, we suppose the problem is

$$\begin{cases} u \in V \\ a(u, v) = \langle f, v \rangle, \forall v \in V \end{cases} \tag{56}$$

where V is the function in Banach space defined on domain Ω. Function $a(\cdot, \cdot)$ and $f \in V'$ satisfy the conditions of the Lax-Milgram theorem.

In space $V_M = \text{span}\{\Phi_i | 1 \le i \le N\} \subset V$, the EFG method for Eq. (56) is

$$\begin{cases} u^M \in V_M, \\ a(u^M, v^M) = \langle f, v^M \rangle, \forall v^M \in V_M \end{cases} \tag{57}$$

We consider the error of $u - u^M$ under the L^2 error norm. Using linear basis function, cubic spline weight function and penalty method, the error and related error of L^2 error norm are defined as follows

$$\|u - u^M\|_{L^2(\Omega)} = \left(\int_\Omega (u - u^M)^2 d\Omega\right)^{\frac{1}{2}} \text{ and} \tag{58}$$

$$\|u - u^M\|^{rel}_{L^2(\Omega)} = \frac{\|u - u^M\|_{L^2(\Omega)}}{\|u\|_{L^2(\Omega)}} \tag{59}$$

By varying the number of nodes and the scaling factor, the convergence study of a 3D solid is studied. We consider the stretching of a prismatic bar by its own weight; if ρg is the weight per unit volume of the bar (Fig. 2), then the body force is

$$X = Y = 0, \quad Z = -\rho g \tag{60}$$

The differential equation of equilibrium is satisfied by letting

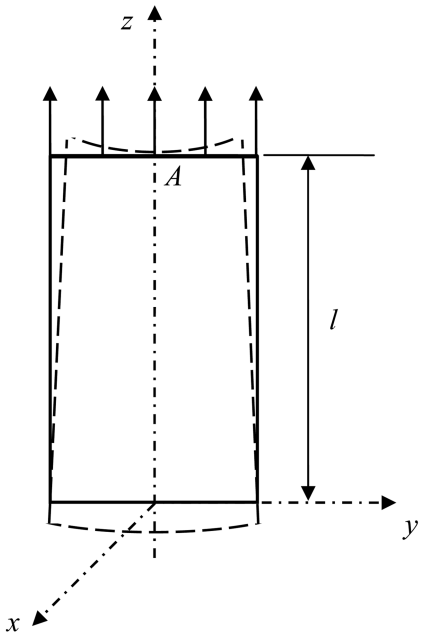

Fig. 2 Stretching a prismatic bar by its own weight

Table 1 Relationship between the number of nodes and the relative error norm (displacement) for the EFG and IEFG methods and their computation time in 4.1

Number of nodes	Relative error norm (displacement)	Computation time of the IEFG method (*s*)	Computation time of the EFG method (*s*)
$5 \times 5 \times 3$	0.0011	19.640	20.328
$5 \times 5 \times 5$	3.0312×10^{-4}	83.063	84.766
$5 \times 5 \times 7$	1.8114×10^{-4}	190.422	191.546
$5 \times 5 \times 9$	1.1255×10^{-4}	311.312	313.750
$5 \times 5 \times 11$	7.5606×10^{-5}	433.078	439.344

$$\sigma_z = \rho g z, \quad \sigma_x = \sigma_y = \tau_{xy} = \tau_{yz} = \tau_{xz} = 0 \tag{61}$$

and assuming that on each cross section, we have uniform tension produced by the weight of the lower potential of the bar. The parameters are taken as $l = 40$ mm, $\nu = 0.15$, $E = 2.069 \times 10^4$ MPa, and $\rho = 2405$ kg/m^3. The final expressions for the displacements are

$$u(x, y, z) = -\frac{\nu \rho g x z}{E} \tag{62}$$

$$v(x, y, z) = -\frac{\nu \rho g y z}{E} \text{ and} \tag{63}$$

$$w(x, y, z) = \frac{\rho g}{2E}(z^2 - l^2) + \frac{\nu \rho g}{2E}(x^2 + y^2) \tag{64}$$

Tables 1 and 2 indicate that under a certain d_{max}, the relative error norm decreases as the number

Table 2 Relationship between the number of nodes and the relative error norm (stress) for the EFG and IEFG methods and their computation time in 4.1

Number of nodes	Relative error norm (stress)	Computation time of the IEFG method (s)	Computation time of the EFG method (s)
$5 \times 5 \times 3$	0.012	23.907	24.953
$5 \times 5 \times 5$	0.0072	112.891	115.125
$5 \times 5 \times 7$	0.0047	254.516	258.110
$5 \times 5 \times 9$	0.0032	416.281	421.500
$5 \times 5 \times 11$	0.0024	579.453	587.484

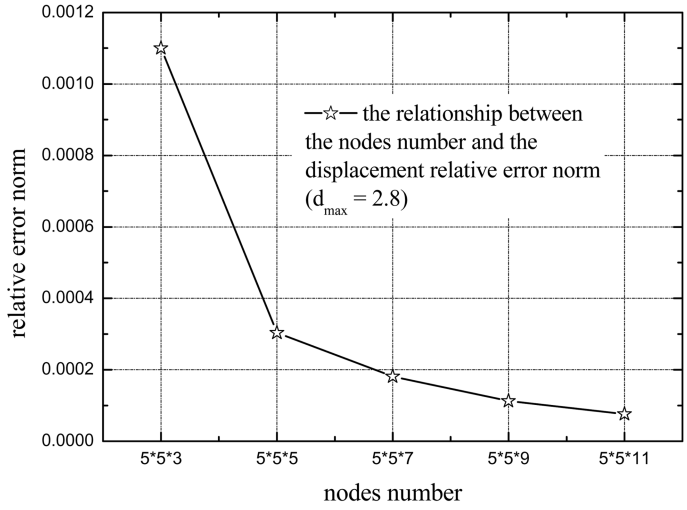

Fig. 3 Convergence rate for displacement with IEFG method and fixed d_{max}

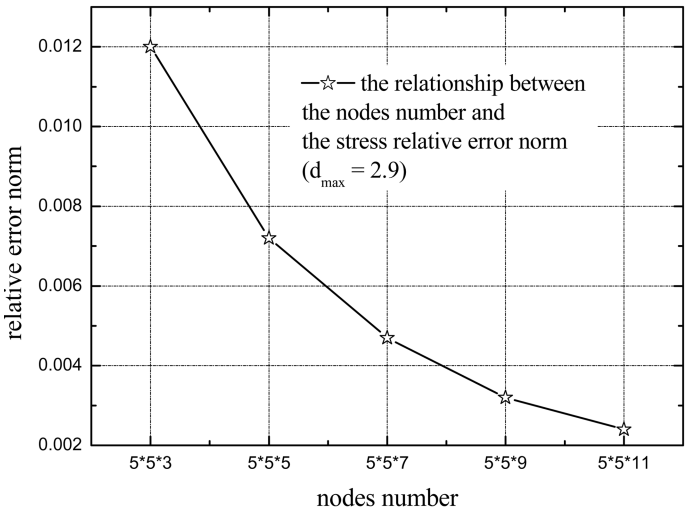

Fig. 4 Convergence rate for stress with IEFG method

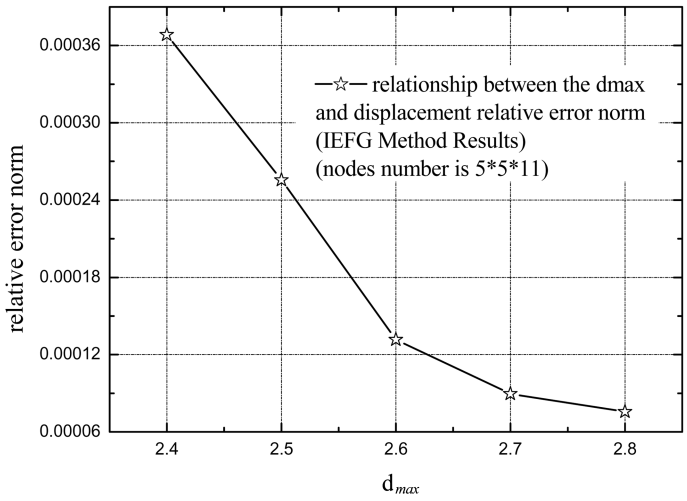

Fig. 5 Convergence rate for displacement with IEFG method and a certain number of nodes

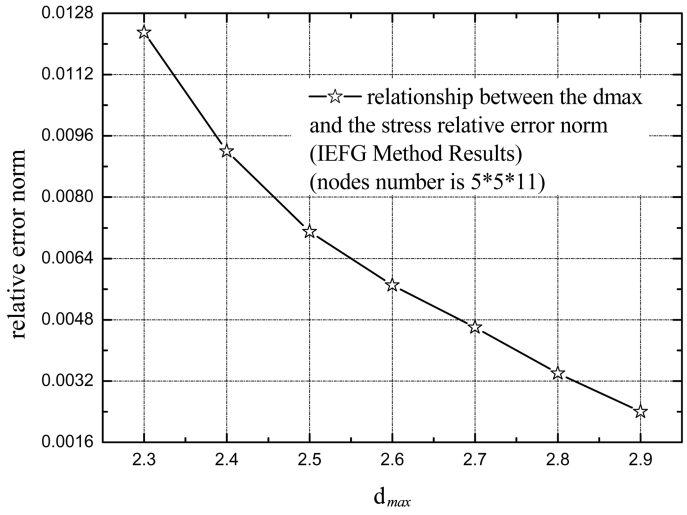

Fig. 6 Convergence rate for stress with IEFG method

of nodes increases and the solution converges when the number of nodes is $5 \times 5 \times 11$. The convergence studies are also plotted in Figs. 3 and 4 to show a clearer convergence trend. From the tables and figures, we conclude that a higher completeness order of the basis function achieves a better convergence rate than the lower order.

In Figs. 5 and 6, we show the convergence of the IEFG method by keeping the number of nodes unchanged and resized the values of d_{max}. Because the proposed method is sensitive to the support size of the nodes that are denoted by the scaling factor, the relative error norm decreases with an increase in d_{max}. It is found that $d_{max} = 2.8$ for the displacement and $d_{max} = 2.9$ for the stress produce good results. In Table 3, we compare the computation time for both EFG and IEFG methods. We

Table 3 Relationship between d_{max} and the relative error norm for the EFG and IEFG methods and their computation time in 4.1

	Relative error norm (displacement)	Relative error norm (stress)	Computation time of the IEFG method (s)	Computation time of the EFG method (s)
2.3	3.6285×10^{-4}	0.0123	242.797	254.422
2.4	3.6828×10^{-4}	0.0092	244.047	259.937
2.5	2.5552×10^{-4}	0.0071	436.219	440.094
2.6	1.3157×10^{-4}	0.0057	434.235	449.594
2.7	8.9576×10^{-4}	0.0046	433.500	442.313
2.8	7.5606×10^{-4}	0.0034	433.078	439.344
2.9	8.5423×10^{-4}	0.0024	579.453	587.484

observe that the IEFG method achieves a faster computational speed with the same precision.

4.2 Example problems

The implementation of the IEFG method for elastostatic problems is now evaluated via a number of examples.

A regular arrangement of nodes and the background mesh of cells are used for the numerical integrations to compute the system equation. In each integration cell, a $3 \times 3 \times 3$ Gauss quadrature scheme is used to evaluate the stiffness matrix. The 3D linear basis function and cubic spline weight function are used in the IMLS approximation.

4.2.1 Load distributed over a part of the boundary of a semi-infinite solid

Imagine that the plane $z = 0$ is the boundary of a semi-infinite solid, and we find the displacements and stresses produced by a distributed load (see Fig. 7). Suppose that ρg is the weight per unit volume of the body, the body forces are $X = Y = 0$, $Z = -\rho g$ and the stress distribution is given by the following equations

$$\sigma_x = \sigma_y = -\frac{\nu}{1-\nu}(q + \rho g z) \tag{65}$$

$$\sigma_z = -(q + \rho g z) \text{ and} \tag{66}$$

$$\tau_{xy} = \tau_{yz} = \tau_{zx} = 0 \tag{67}$$

The vertical displacement of the semi-infinite body is

$$w = \frac{(1+\nu)(1-2\nu)}{E(1-\nu)}\left[q(h-z) + \frac{\rho g}{2}(h^2 - z^2)\right] \tag{68}$$

The parameters are $q = 1$ MPa, $E = 2.069 \times 10^4$ MPa, $\nu = 0.15$, and $\rho = 2405$ kg/m^3.

Figs. 8 and 9 present the analytical solution and numerical results by using the EFG and IEFG methods. It can be seen that when $d_{max} = 2.0$ for displacement and $d_{max} = 2.7$ for stress, both methods works well; however, the computational speed of the IEFG method is faster than that of the EFG method.

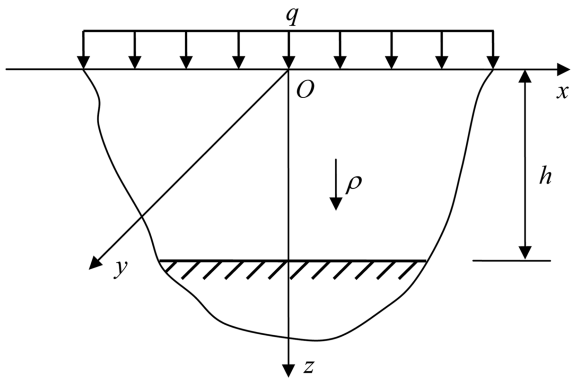

Fig. 7 Load distributed over a part of the boundary of a semi-infinite solid

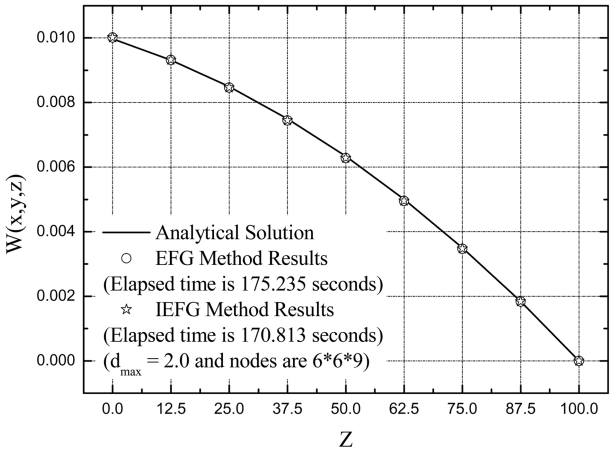

Fig. 8 Displacement distribution along *Z* axis

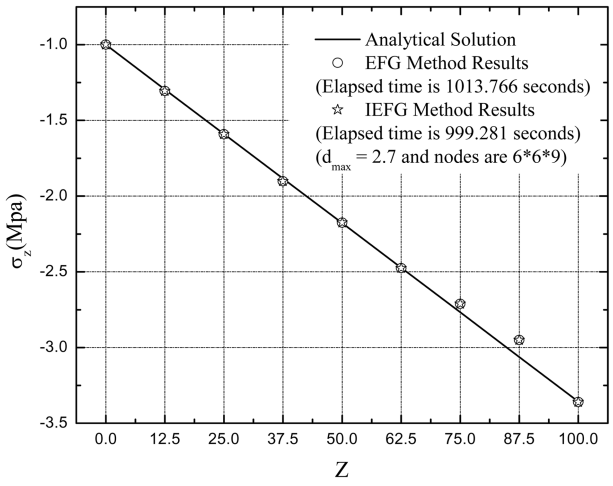

Fig. 9 Normal stress distribution along *Z* axis

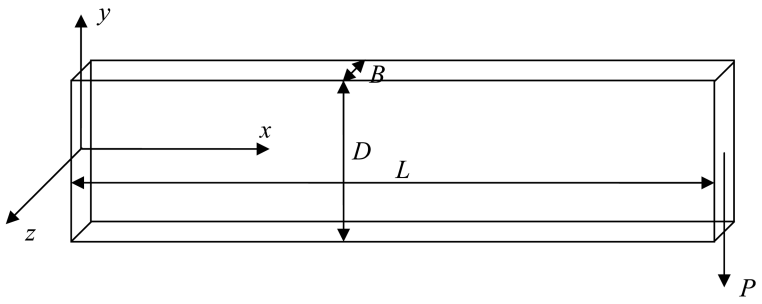

Fig. 10 3D cantilever beam subjected to a parabolic at the free end

4.2.2 A cantilever beam

The 3D cantilever beam, shown in Fig. 10, is investigated to benchmark the proposed method. The left end of the beam is fixed, and the right end is subjected to paraboloidally distribute downward traction. As the beam is relatively thin, a plane stress problem can be considered to yield the analytical solution. This analytical solution is then adopted as the reference value in our numerical study.

The displacement components of the analytical solution are given by

$$u_x = -\frac{py}{6EI}\left[(6L-3x)x+(2+\nu)\left(y^2-\frac{D^2}{4}\right)\right] \text{ and} \tag{69}$$

$$u_y = \frac{py}{6EI}\left[3\nu y^2(L-x)+(4+5\nu)\frac{D^2x}{4}+(3L-x)x^2\right] \tag{70}$$

where the moment of the inertia I of the beam is given by $I = D^3/12$, $\nu = 0.3$ and $E = 30\text{MPa}$. The stress components that correspond to the foregoing displacements are

$$\sigma_x = -\frac{p(L-x)y}{I} \tag{71}$$

$$\sigma_y = 0 \text{ and} \tag{72}$$

$$\sigma_{xy} = \frac{p}{2I}\left(\frac{D^2}{4}-y^2\right) \tag{73}$$

The parameters are taken as $p = -1000$, $L = 50$, $D = 12$, and $B = 1$ in the study of this numerical example.

Figs. 11-13 show the comparisons between the EFG, IEFG results and the analytical solutions, in which Fig. 11 shows the comparison for displacement in y-direction along the neutral axis, Fig. 12 for the normal stress and Fig. 13 for the shear stress. All these plots show that the results obtained using both EFG and IEFG methods are in good agreement with the analytical solutions, yet about five percent of the computation time is saved with IEFG method.

4.2.3 3D Lame problem

The three-dimensional Lame problem consists of a hollow sphere, with inner and outer radius a and b, respectively, under internal pressure. Fig. 14 shows a schematic of the problem under

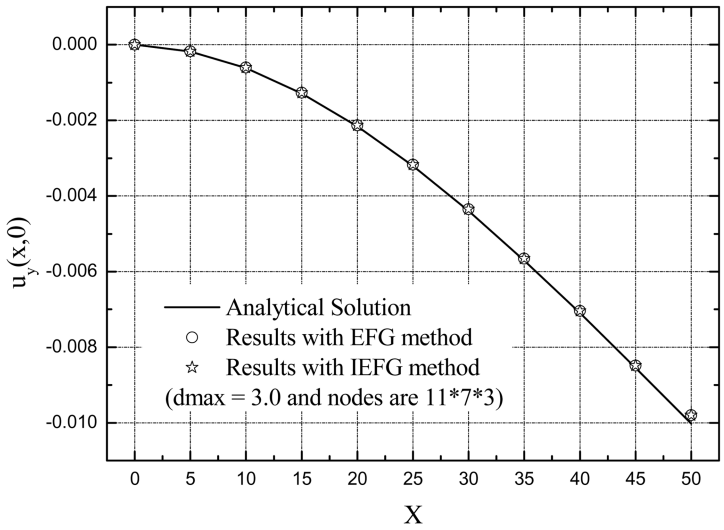

Fig. 11 Displacement (u_y) distribution along the neutral axis

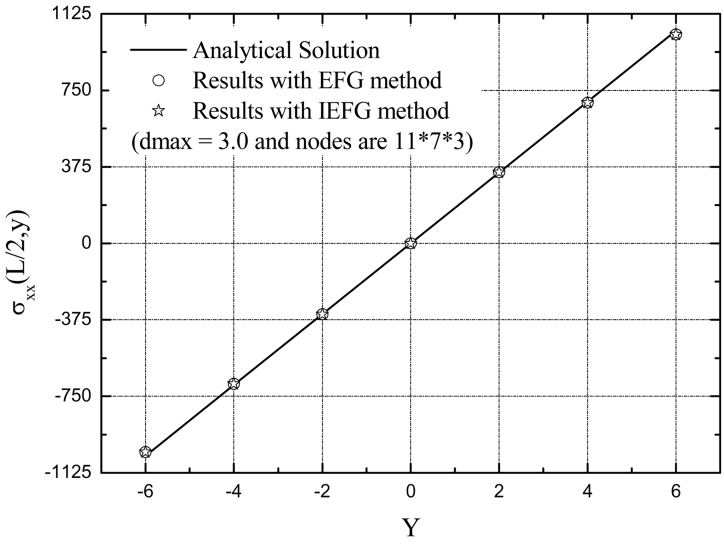

Fig. 12 Normal stress distribution along the line of $x = L/2$, $z = 0.0$

consideration. The numerical solution for this problem is obtained using the material parameters $E = 1.0$ and $\nu = 0.25$ and the geometric parameters $a = 10$ and $b = 20$, with an internal pressure $p = 1$.

The exact solutions for the radial displacement and radial and tangential stresses are given as

$$u_r = \frac{pa^3 r}{E(b^3 - a^3)}\left[(1-2\nu) + (1+\nu)\frac{b^3}{2r^3}\right] \tag{74}$$

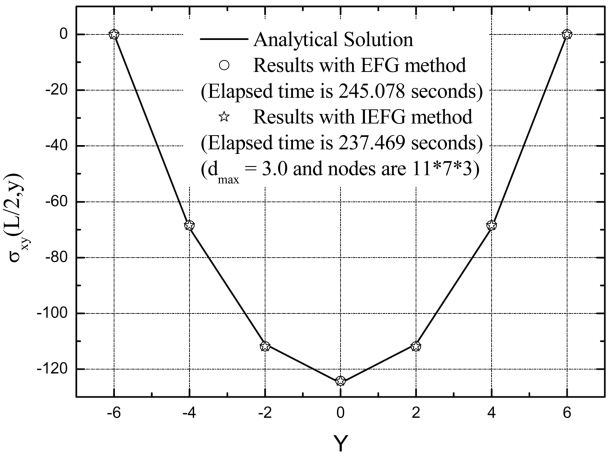

Fig. 13 Shear stress distribution along the line of $x = L/2$, $z = 0.0$

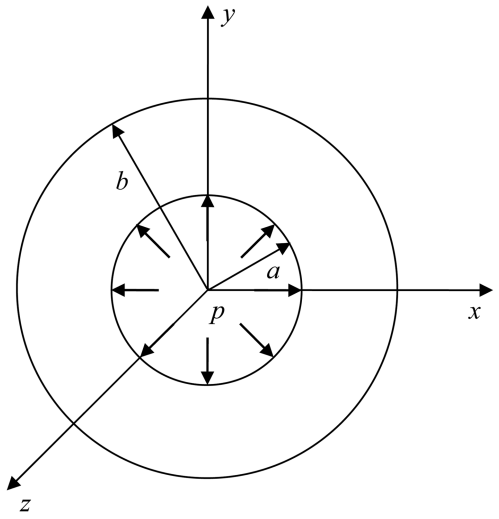

Fig. 14 3D Lame problem: hollow sphere under internal pressure

$$\sigma_r = -\frac{\frac{b^3}{r^3} - 1}{\frac{b^3}{a^3} - 1} \tag{75}$$

$$\sigma_\theta = -\frac{\frac{b^3}{2r^3} + 1}{\frac{b^3}{a^3} - 1} p \tag{76}$$

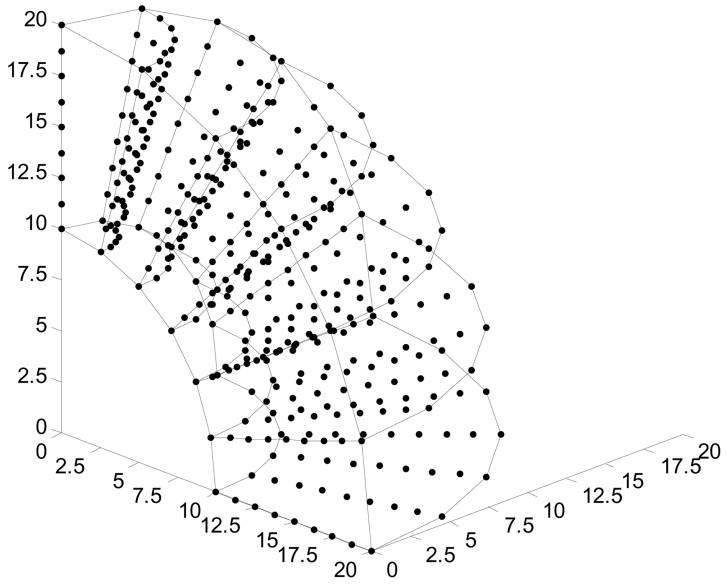

Fig. 15 One eighth of a hollow sphere and nodes arrangement

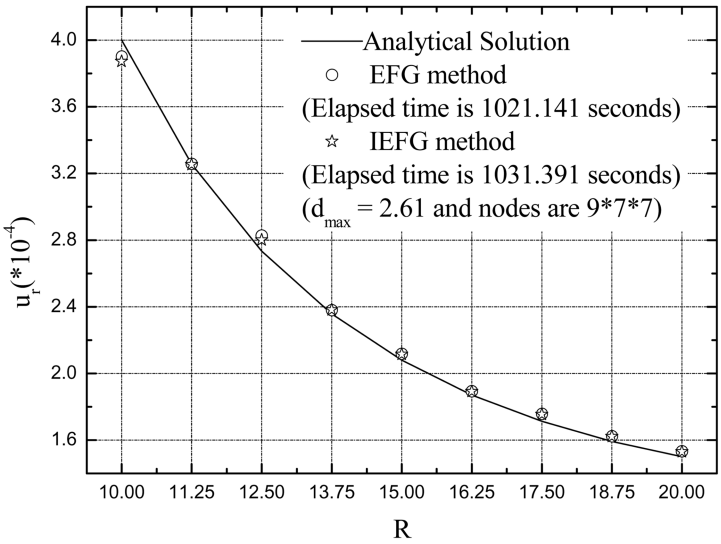

Fig. 16 Radial displacement u_r on the hollow sphere

Due to the symmetry of the hollow sphere and inner pressure, one eighth of the hollow sphere is considered when the EFG and IEFG methods are used. Fig. 15 shows the nodes distribution of the problem domain. The displacement and stress that are obtained using both the EFG and IEFG methods are shown in Figs. 16 and 17. It should be noted that in this analysis, the same number of nodes but different d_{max} are used for displacement and stress. As the figures shown, the computational time elapsed by IEFG method is slightly less than the EFG method.

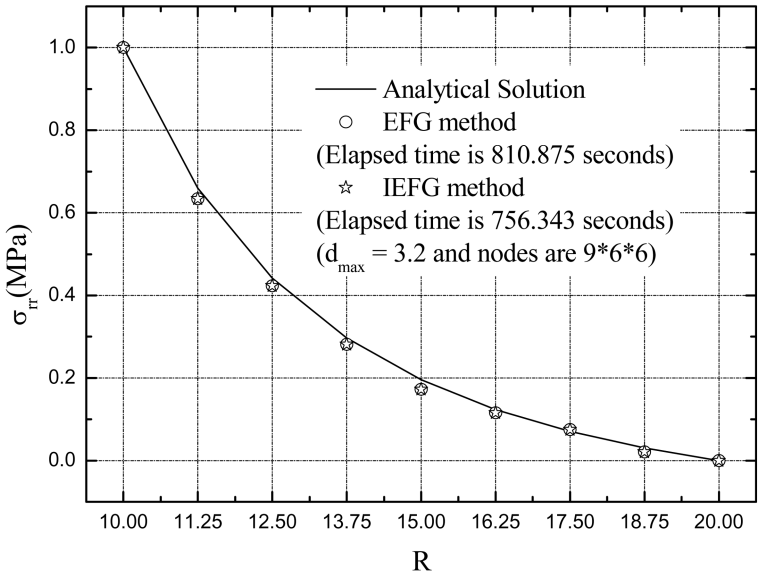

Fig. 17 The stress σ_r on the hollow sphere

5. Conclusions

This paper proposes an IEFG method that is based on IMLS. By comparing example results obtained with the EFG and the analytical solution, it has been demonstrated that the IEFG method is efficient for dealing with 3D elastic problems. In IMLS approximation, the orthogonal function system with a weight function is used as the basis function. IMLS approximation has greater computational efficiency and precision than does MLS approximation, and it also does not lead to an ill-conditioned system of equations. This means that this system can be solved without obtaining the inverse matrix, and fewer coefficients are involved. The method has been demonstrated for solving several example problems and concluded that the convergence rate of IEFG method is slightly better than the EFG method.

References

Atluri, S.N. and Zhu, T.L. (1998), "A new meshless local Petrov-Galerkin (MLPG) approach in computational mechanics", *Comput. Mech.*, **22**, 117-127.

Belytschko, T., Krongauz, Y., Organ, D., Fleming, M. and Krysl, P. (1996), "Meshless method: an overview and recent developments", *Comput. Meth. Appl. Mech. Eng.*, **139**, 3-47.

Belytschko, T., Lu, Y.Y. and Gu, L. (1994), "Element-free Galerkin methods", *Int. J. Numer. Meth. Eng.*, **37**, 229-256.

Duarte, C.A. and Oden, J.T. (1995), "Hp clouds-a meshless method to solve boundary-value problems", Technical report 95-05, Texas Institute for Computational and Applied Mathematics, University of Texas at Austin.

Hu, H.Y., Lai, C.K. and Chen, J.S. (2009), "A study on convergence and complexity of reproducing kernel collocation method", *Interaction Multiscale Mech.*, **2**(3), 295-319.

Kitipornchai, S., Liew, K.M. and Cheng, Y. (2005), "A boundary element-free method (BEFM) for three-dimensional elasticity problems", *Computat. Mech.*, **36**, 13-20.
Lancaster, P. and Salkauskas, K. (1981), "Surface generated by moving least squares methods", *Math. Comput.*, **37**, 141-158.
Liew, K.M, Huang, Y.Q. and Reddy, J.N. (2003), "Moving least-squares differential quadrature method and its application to the analysis of shear deformable plates", *Int. J. Numer. Meth. Eng.*, **56**, 2331-2351.
Liew, K.M. and Chen, X.L. (2004a), "Mesh-free radial basis function method for buckling analysis of non-uniformly loaded arbitrarily shaped shear deformable plates", *Comput. Meth. Appl. Mech. Eng.*, **193**, 205-224.
Liew, K.M. and Chen, X.L. (2004b), "Mesh-free radial point interpolation method for the buckling analysis of Mindlin plates subjected to in-plane point loads", *Int. J. Numer. Meth. Eng.*, **60**, 1861-1877.
Liew, K.M. and Chen, X.L. (2004c), "Buckling of rectangular Mindlin plates subjected to partial in-plane edge loads using the radial point interpolation method", *Int. J. Solids Struct.*, **41**, 1677-1695.
Liew, K.M., Cheng Yumin, and Kitipornchai, S. (2006), "Boundary element-free method (BEFM) and its application to two-dimensional elasticity problems", *Int. J. Numer. Meth. Eng.*, **65**(8), 1310-1332.
Liew, K.M., Cheng, Y. and Kitipornchai, S. (2005), "Boundary element-free method (BEFM) for two-dimensional elastodynamic analysis using Laplace transform", *Int. J. Numer. Meth. Eng.*, **64**, 1610-1627.
Liew, K.M., Feng, C., Cheng, Y. and Kitipornchai, S. (2007), "Complex variable moving least-squares method: A meshless approximation technique", *Int. J. Numer. Meth. Eng.*, **70**, 46-70.
Liew, K.M., Huang, Y.Q. and Reddy, J.N. (2004), "Analysis of general shaped thin plates by the moving least-squares differential quadrature method", *Finite Elem. Anal. Des.*, **40**, 1453-1474.
Liu, G.R., *Mesh free methods: moving beyond the finite element method*, Boca Raton, FL: CRC Press LLC.
Liu, W.K., Jun, S. and Zhang, Y.F. (1995), "Reproducing kernel particle method", *Int. J. Numer. Meth. Fl.*, **20**, 1081-1106.
Matsubara, H. and Yagawa, G. (2009), "Convergence studies for Enriched Free Mesh Method and its application to fracture mechanics", *Interaction Multiscale Mech.*, **2**(3), 277-293.
Nayroles, B., Touzot, G. and Villon, P.G. (1992), "Generalizing the finite element method: diffuse approximation and diffuse elements", *Comput. Mech.*, **10**, 307-318.
Sun, Y.Z., Zhang, Z., Kitipornchai, S. and Liew, K.M. (2006), "Analyzing the interaction between collinear interfacial cracks by an efficient boundary element-free method", *Int. J. Eng. Sci.*, **44**, 37-48.
Wang, D. and Wu, Y. (2008), "An efficient Galerkin meshfree analysis of shear deformable cylindrical panels", *Interaction Multiscale Mech.*, **1**(3), 339-355.
Wu, C.T. and Koishi, M. (2009), "A Meshfree procedure for the microscopic analysis of particle-reinforced rubber compounds", *Interaction Multiscale Mech.*, **2**(2), 129-151.